

DEVELOPMENT OF CURVED-PLATE ELEMENTS FOR THE EXACT BUCKLING ANALYSIS OF COMPOSITE PLATE ASSEMBLIES INCLUDING TRANSVERSE SHEAR EFFECTS

David M. McGowan*
NASA Langley Research Center
Hampton, VA 23681-0001

and

Melvin S. Anderson**
Eagle Aeronautics, Inc.
Newport News, VA 23606

Abstract

The analytical formulation of curved-plate non-linear equilibrium equations that include transverse-shear-deformation effects is presented. A unified set of non-linear strains that contains terms from both physical and tensorial strain measures is used. Using several simplifying assumptions, linearized, stability equations are derived that describe the response of the plate just after bifurcation buckling occurs. These equations are then modified to allow the plate reference surface to be located a distance z_c from the centroidal surface which is convenient for modeling stiffened-plate assemblies. The implementation of the new theory into the VICONOPT buckling and vibration analysis and optimum design program code is described. Either classical plate theory (CPT) or first-order shear-deformation plate theory (SDPT) may be selected in VICONOPT. Comparisons of numerical results for several example problems with different loading states are made. Results from the new curved-plate analysis compare well with closed-form solution results and with results from known example problems in the literature. Finally, a design-optimization study of two different cylindrical shells subject to uniform axial compression is presented.

List of Symbols

A	extensional stiffness matrix		resultants
a	upper half of the eigenvectors of matrix R , associated with displacements	m_{11}, m_{22}, m_{12}	perturbation values of moment resultants just after buckling has occurred
B	coupling stiffness matrix	$\tilde{m}_{11}, \tilde{m}_{22}, \tilde{m}_{12}$	moment resultants
B, C, E,		N_{11}, N_{22}, N_{12}	applied (prebuckling) stress resultants
F, G, H	coefficients used to select physical or tensorial strains	n_{11}, n_{22}, n_{12}	perturbation values of stress resultants just after buckling has occurred
b	lower half of the eigenvectors of matrix R , associated with forces	$\tilde{n}_{11}, \tilde{n}_{22}, \tilde{n}_{12}$	stress resultants
b	plate width (arc length)	$\hat{n}_{22}, \hat{n}_{12}$	effective forces per unit length at an edge $\xi_2 = \text{constant}$
c	single eigenvector of matrix R	n_1	number of layers in a general curved laminate
D	bending stiffness matrix	P	coefficient matrix of the set of first-order plate differential equations
d	vector of displacement amplitudes at the two edges of a plate	$\bar{\mathbf{Q}}$	lamina reduced transformed stiffness matrix
E_{ii}	Young's modulus in the i-direction	Q_1, Q_2	applied (prebuckling) shear stress resultants
E	matrix used to define vector d	$q_1, q_2,$	perturbation values of shear stress resultants just after buckling has occurred
F	matrix used to define vector f	\tilde{q}_1, \tilde{q}_2	shear stress resultants
f	vector of force amplitudes at the two edges of a plate	\hat{q}_2	effective transverse shear force per unit length at an edge $\xi_2 = \text{constant}$
G_{ij}	shear stiffness associated with i-j direction	R	matrix whose eigenvalues are the characteristic roots of the plate differential equations
I	identity matrix	R_1, R_2	radii of lines of principal curvature
i	imaginary number, square root of -1	T	coefficient matrix of the set of first-order plate differential equations
K	plate stiffness matrix	t	plate thickness
k	transverse shear compliance matrix	U_1, U_2	prebuckling displacements
M_{11}, M_{22}, M_{12}	applied (prebuckling) moment	u_1, u_2	perturbation values of displacements just after buckling has occurred

* Aerospace Engineer, Structural Mechanics Branch, Structures Division. Senior Member, AIAA.

** Research Engineer. Associate Fellow, AIAA.

w	normal displacement in the ξ_3 -direction
\mathbf{Z}	vector of the forces and displacements in the plate
\mathbf{z}	vector of the amplitudes of the forces and displacements in the plate assuming a sinusoidal variation in the ξ_1 -direction
z_c	distance from the plate centroidal surface to the plate reference surface
z_k	distance from laminate reference surface to the k th layer in the laminate

Greek

α_1, α_2	Lamé parameters
β	angle included by a curved plate
$\boldsymbol{\varepsilon}$	vector containing strains ε_{11} , ε_{22} , and γ_{12}
$\varepsilon_{11}, \varepsilon_{22}$	in-plane direct strains
$\varepsilon_{12}, \gamma_{12}$	in-plane shear strains
$\varepsilon_{13}, \gamma_{13}$	
$\varepsilon_{23}, \gamma_{23}$	transverse shear strains
ϕ_1, ϕ_2	rotations
ϕ_n	rotation about the normal to the plate middle surface
\mathbf{k}	vector containing curvatures κ_{11} , κ_{22} , and κ_{12}
κ_{11}, κ_{22}	middle surface changes in curvature
κ_{12}	middle surface twisting curvature
λ	half wavelength of buckling mode
ν	Poisson's ratio
θ_k	angular orientation of ply k in a laminate with respect to the laminate coordinate system
ρ	density
$\boldsymbol{\sigma}$	vector containing stresses σ_{11} , σ_{22} , and τ_{12}
σ_{11}, σ_{22}	in-plane direct stresses
τ_{12}	in-plane shear stress
ξ_1, ξ_2, ξ_3	coordinate measures in the 1, 2, and 3-directions, respectively

Subscripts and Superscripts

cr	critical value for buckling
k	k th layer in a laminated composite plate
n	normal to middle surface
1, 2, 3	1, 2, and 3-directions, respectively
$^{\circ}$	value at centroidal surface

Introduction

Longitudinally stiffened plate structures occur frequently in aerospace vehicle structures. Thus, analysis and optimization capabilities that can be used economically for their design are of great importance. One approach to modeling these structures is to represent the stiffened panel mathematically by long, thin, flat or curved-plate elements that are rigidly connected along their longitudinal edges as shown in Figure 1. Furthermore, the designs for these structures

often exploit the increased structural efficiency that can be obtained by the use of advanced composite materials. Therefore, any analysis tool used to design these structures must include the effects of anisotropy and through-the-thickness or transverse-shear deformation. The transverse-shear deformation capability is especially important when the plate elements are thick compared to their width or are made of compliant lamina. Additionally, to satisfy the current demands for more cost-effective and structurally efficient aerospace vehicles, these structures are frequently optimized to obtain minimum-mass designs that satisfy a wide range of constraints. Two particularly important phenomena that must be accounted for when performing a design optimization of a stiffened-plate structure are buckling and vibration. Constraints on buckling loads, vibration frequencies, or a combination of both usually appear as design criteria in the design-optimization process. Therefore, an analytical tool that is economical and predicts accurately the structural response of stiffened-plate structures is highly desirable. One such analytical tool is the VICONOPT computer code [1].

The VICONOPT computer code is an analysis and design-optimization code for the buckling and vibration analyses of prismatic assemblies of flat- or curved-plate elements subjected to in-plane-loads. The code includes the capability to model anisotropic stiffened-plate structures that have fully populated \mathbf{A} , \mathbf{B} and \mathbf{D} stiffness matrices. The user can select either classical plate theory (CPT) or first-order transverse-shear-deformation plate theory (SDPT) [2]. The SDPT used in VICONOPT and in the present study uses the usual first-order assumption that straight material lines that are originally normal to the centroidal surface of a plate remain straight and inextensional during deformation of the plate, but not necessarily normal to the centroidal surface. The formulation used in VICONOPT to model plate elements is referred to herein as an exact finite-strip method (FSM) [3] because it uses the exact solution to the differential equations that describe the behavior of a plate element to formulate the corresponding stiffness matrices. Examples of other exact FSM analyses of curved plates are given in Refs. [4, 5, and 6]. Other FSM analyses that formulate the stiffness matrices from a variational approach are referred to as approximate FSM's. Examples of approximate FSM analyses of curved plates are given in Refs. [7 and 8].

As the use of advanced composite materials has increased in the design of aerospace vehicles, stiffened-plate structures with one or more curved-plate elements have become more common. Currently, the VICONOPT code approximates the geometry of a

curved plate by subdividing or discretizing it into a series of flat-plate elements that are joined to form the complete curved plate as shown in Figure 2. Thus, the analyst must ensure that an adequate number of flat-plate elements is used in the analysis. This procedure is analogous to the discretization approach used in finite element analysis, and it is referred to herein as the segmented-plate analysis in the VICONOPT code. Although this approach is not very difficult, it would be more efficient to have an exact method for modeling curved-plate elements within VICONOPT.

The present paper describes an analysis method for modeling curved-plate elements exactly that has been implemented into the VICONOPT code. This new analysis capability is referred to herein as the curved-plate analysis in VICONOPT. Several features accompanying this analysis that have been added to the VICONOPT code are described in the present paper. The current version of VICONOPT only analyzes flat-plate elements based on a tensorial strain-displacement relation. However, the choice of strain-displacement relations can affect the magnitude and distribution of prebuckling stresses in curved plates. Therefore, a unified set of nonlinear strain-displacement relations that contains terms from both physical and tensorial strain measures is used to derive the curved-plate equilibrium equations. This unified set of strains is used throughout the derivation of the equilibrium equations, and the selection of either physical or tensorial strains is achieved by setting appropriate coefficients in the equilibrium equations equal to one or zero. Another addition to the code is the option to include the effects of in-plane transverse loads that act perpendicular to the longitudinal edges of a plate element and in-plane shear loads in the in-plane equilibrium equations. These effects are currently ignored in the VICONOPT code (see [1]). All of these features have been implemented such that they are available for use in the analysis of both flat and curved-plate elements. The methodology used to accomplish this enhancement of the code and results obtained using this new capability are presented.

Analytical Formulation

The analytical formulation of the present theory is described. The geometry, loadings, and sign conventions used in the present study are described first. The unified set of strain-displacement relations used in the present theory is then presented. Next, the derivation of a set of non-linear equilibrium equations and linearized stability equations is described. The stability equations are then modified such that they describe the response of the curved-plate segment with

respect to a reference surface which may be offset from the centroidal surface of the plate. These modified stability equations are needed to simplify the numerical procedure used to implement the present analysis into the VICONOPT code.

Geometry, Loadings, and Sign Conventions

The geometry of the basic curved-plate element this is being studied in this section is given in Figure 3. This figure depicts the orthogonal curvilinear coordinate system (ξ_1, ξ_2, ξ_3) used in the analysis. The ξ_1 - and ξ_2 -axes shown in the figure are along lines of principal curvature and they have radii of curvature R_1 and R_2 , respectively. Lines of principal curvature coordinates are sufficient for the analysis because twist of the curved-plate reference surface is absent in prismatic curved-plate assemblies. The reference surface for a curved-plate element used herein is its middle surface, and the corresponding first fundamental form is given by

$$ds^2 = \alpha_1^2 d\xi_1^2 + \alpha_2^2 d\xi_2^2 \quad (1)$$

where α_1 and α_2 are the Lamé parameters. The coordinates ξ_1 and ξ_2 are measured as arc lengths along the ξ_1 - and ξ_2 -axes, respectively. The result of measuring the coordinates in this manner is $\alpha_1 = \alpha_2 = 1$. The sign conventions for buckling displacements, moments, rotations, and stress resultants are also shown in Figure 3. The sign convention for the applied in-plane loadings and the relationship of the reference surface of the plate to the centroidal surface of the plate are shown in Figure 4. The centroidal surface is defined to be located at the centroid of the face of the panel that is normal to the ξ_1 -axis. Observe that the centroidal surface can be offset from the reference surface by a distance z_c . This offset is useful in maintaining a smooth outer-surface mold line when plates of different thicknesses are linked together (as in the analysis of a stringer-stiffened panel). The loading N_{22} shown in Figure 4 is referred to in the present paper as an in-plane transverse loading.

Strain-Displacement Relations

The unified set of nonlinear strain-displacement relations used for the present study for small strains are given by

$$\begin{aligned} \epsilon_{11} = & u_{1,1} + \frac{w}{R_1} + \frac{1}{2} \left[w_{,1} - \frac{u_1}{R_1} \right]^2 \\ & + \frac{B}{2} (u_{2,1})^2 + \frac{C}{2} \left[u_{1,1} + \frac{w}{R_1} \right]^2 \end{aligned} \quad (2a)$$

$$\varepsilon_{22} = u_{2,2} + \frac{w}{R_2} + \frac{1}{2} \left[w_{,2} - \frac{u_2}{R_2} \right]^2 \quad (2b)$$

$$+ \frac{E}{2} (u_{1,2})^2 + \frac{F}{2} \left[u_{2,2} + \frac{w}{R_2} \right]^2$$

$$2\varepsilon_{12} = \gamma_{12} = u_{1,2} + u_{2,1} + w_{,1} w_{,2} - w_{,1} \frac{u_2}{R_2} - w_{,2} \frac{u_1}{R_1} + \frac{u_1 u_2}{R_1 R_2} - \underline{G} [u_{1,2} u_{2,2} + u_{2,1} u_{1,1}] \quad (2c)$$

$$+ u_{1,2} \frac{w}{R_2} + u_{2,1} \frac{w}{R_1} + \underline{H} [u_{1,2} u_{1,1} + u_{2,1} u_{2,2} + u_{1,2} \frac{w}{R_1} + u_{2,1} \frac{w}{R_2}]$$

$$2\varepsilon_{13} = \gamma_{13} = w_{,1} - \frac{u_1}{R_1} - \phi_1 \quad (2d)$$

$$2\varepsilon_{23} = \gamma_{23} = w_{,2} - \frac{u_2}{R_2} - \phi_2 \quad (2e)$$

where the following notation for partial derivatives is used: $\frac{\partial u_i}{\partial \xi_j} \equiv u_{i,j}$. The displacement quantities in Eqs.

(2a)-(2e) are displacements of the centroidal surface of the curved-plate element. The constants \underline{B} , \underline{C} , \underline{E} , \underline{F} , and \underline{H} are set equal to one and \underline{G} is set equal to zero in Eqs. (2a)-(2c) to obtain tensorial strain measures. The constants \underline{B} , \underline{E} , and \underline{G} are set equal to one and \underline{C} , \underline{F} , and \underline{H} are set equal to zero to obtain physical strain measures. Note that the linear portions of the tensorial and physical strain measures are identical. The tensorial strain measures are those of Novozhilov [9]. The physical strains used in the present thesis are derived in a manner similar to that presented by Stein in [10] and they were communicated to the first author in terms of lines of curvature coordinates by Dr. Michael P. Nemeth¹.

The definitions for the changes in curvature of the centroidal surface in terms of surface rotations used for both theories are

$$\kappa_{11} = -\phi_{1,1} \quad (3a)$$

$$\kappa_{22} = -\phi_{2,2} \quad (3b)$$

$$\kappa_{12} = -(\phi_{1,2} + \phi_{2,1}) \quad (3c)$$

These changes in curvatures are equivalent to those given by Sanders in [11] with the terms involving

¹ Structures Division, Structural Mechanics Branch, NASA Langley Research Center, Hampton, Virginia, 23681-0001

rotations about the normal neglected to simplify the analysis.

Derivation of Stability Equations

The nonlinear equilibrium equations for the curved plate illustrated in Figure 3 are derived using the principle of virtual work [12]. The present derivation uses the principle of virtual work in the manner of Sanders [13] that is written in the following form

$$\iint_{\text{area}} \left[\tilde{n}_{11} \delta \varepsilon_{11} + \tilde{n}_{22} \delta \varepsilon_{22} + 2\tilde{n}_{12} \delta \varepsilon_{12} + \tilde{m}_{11} \delta \kappa_{11} + \tilde{m}_{22} \delta \varepsilon_{22} + 2\tilde{m}_{12} \delta \kappa_{12} + \tilde{q}_1 \delta \gamma_{13} + \tilde{q}_2 \delta \gamma_{23} \right] d\xi_1 d\xi_2 + \oint_c \left[N_{11} \delta u_1 + N_{12} \delta u_2 + Q_1 \delta w - M_{11} \delta \phi_1 - M_{12} \delta \phi_2 \right] d\xi_2 - \oint_c \left[N_{12} \delta u_1 + N_{22} \delta u_2 + Q_2 \delta w - M_{12} \delta \phi_1 - M_{22} \delta \phi_2 \right] d\xi_1 = 0 \quad (4)$$

The terms \tilde{n}_{12} and \tilde{m}_{12} are the effective membrane-shear and bending stress measures, respectively, defined by Sanders in [13]. The terms \tilde{q}_1 and \tilde{q}_2 are the effective transverse-shear stress measures defined by Cohen in [14]. The uppercase terms in Eq. (4) are the applied loads on the boundary of the plate.

In order to derive a set of non-linear equilibrium equations that adequately models the behavior of an assembly of curved or flat-plate elements, the issue of continuity of rotations at a plate junction must be examined. When two plates are joined together such that one cross-section is oriented at an arbitrary angle, α , to the other, rotations about the normals to the centroidal surfaces of the two plates must be included to satisfy continuity of rotations. However, this rotation, ϕ_n , has been neglected in the kinematic equations used in the present paper. To account for this effect, a procedure to maintain continuity of rotations that was developed by Cohen in [15] is used in the present study and in VICONOPT. This procedure introduces the shear strain, γ_{13} , as a fundamental displacement variable instead of the rotation, ϕ_1 by replacing ϕ_1 with the expression $w_{,1} - \frac{u_1}{R_1} - \gamma_{13}$ in the

boundary integral over ξ_2 in Eq. (4). Although a detailed discussion of this topic is given in reference [16], a brief discussion of the justification for using this approach is presented subsequently. As shown in reference [16] the equations for continuity of rotations at a plate junction will be satisfied if the transverse shear strain, γ_{13} , equals zero for any non-zero value of the angle α . Therefore, if γ_{13} is a fundamental displacement variable, it may easily be set equal to zero

by simply striking out the appropriate rows and columns in the stiffness matrix of the plate. The equations of continuity of rotations at a plate junction presented in reference [16] also indicate that for $\alpha = 0$, the values of γ_{13} in each plate are equal.

To derive a set of nonlinear equilibrium equations, the variations of Eqs. (2) and (3) are substituted into Eq. (4) and the resulting equation is integrated by parts to yield an integral equation that consists of an area integral and two line integrals. This integral equation is given in reference [16]. Recall that, per Cohen's procedure, ϕ_1 is replaced with the expression

$$w_{,1} - \frac{u_1}{R_1} - \gamma_{13} \quad \text{in the boundary integral over } \xi_2 \text{ in Eq.}$$

(4). For arbitrary displacements u_1 , u_2 , w , ϕ_1 , and ϕ_2 , the coefficients of the displacements in the area integral are the five equilibrium equations. The coefficients of the displacement variables in the line integrals are the natural or force boundary conditions for the edges $\xi_1 = \text{constant}$ and $\xi_2 = \text{constant}$.

A set of linear perturbation equilibrium equations that govern the stability of the plate, referred to herein as the stability or linear bifurcation buckling equations, is obtained by taking the difference between the equilibrium equations evaluated for a stable equilibrium state just prior to bifurcation buckling and an adjacent (perturbed) equilibrium state (not necessarily stable) just after bifurcation buckling has occurred. The prebuckling state is represented herein by:

$$\begin{aligned} \tilde{n}_{11} &= -N_{11}, \quad \tilde{n}_{22} = -N_{22}, \quad \tilde{n}_{12} = -N_{12}, \\ \tilde{m}_{11} &= -M_{11}, \quad \tilde{m}_{22} = -M_{22}, \quad \tilde{m}_{12} = -M_{12}, \quad (5) \\ \tilde{q}_1 &= -Q_1, \quad \tilde{q}_2 = -Q_2, \quad U_1, \quad U_2, \quad W \end{aligned}$$

where the minus signs in the loading terms reflect the sign convention used in which the applied loads are opposite in direction to the loads that develop after buckling. The adjacent equilibrium state just after bifurcation buckling has occurred is represented herein by:

$$\begin{aligned} \tilde{n}_{11} &= n_{11} - N_{11}, \quad \tilde{n}_{22} = n_{22} - N_{22}, \\ \tilde{n}_{12} &= n_{12} - N_{12}, \quad \tilde{m}_{11} = m_{11} - M_{11}, \\ \tilde{m}_{22} &= m_{22} - M_{22}, \quad \tilde{m}_{12} = m_{12} - M_{12}, \quad (6) \\ \tilde{q}_1 &= q_1 - Q_1, \quad \tilde{q}_2 = q_2 - Q_2, \quad u_1 + U_1, \\ u_2 + U_2, \quad w + W \end{aligned}$$

where the lower-case variables are perturbation variables. Taking the difference between the two equilibrium states represented by Eqs. (5) and (6), linearizing the resulting equations with respect to the perturbation variables, and applying several simplifying assumptions yields the set of five stability equations

and two sets of boundary conditions given in reference [16]. These assumptions are:

- 1) Prebuckling deformations, moments and transverse shear stress are negligible
- 2) The in-plane prebuckling stress state is uniform

The form of the stability equations used herein is a form that describes the response of the curved plate with respect to a reference surface of the plate that is located a distance z_c from the centroidal surface shown in Figure 4. To obtain this form of the stability equations, the following information is used:

1) The relationships of the displacements at the centroidal surface, u_1^o and u_2^o , to the displacements at the reference surface, u_1 and u_2 are:

$$u_1^o = u_1 - z_c \phi_1 \quad (7a)$$

$$u_2^o = u_2 - z_c \phi_2 \quad (7b)$$

2) The relationships of the moments at the centroidal surface, m_{11}^o , m_{22}^o , and m_{12}^o , to the displacements at the reference surface, m_{11} , m_{22} , and m_{12} are:

$$m_{11}^o = m_{11} - z_c n_{11} \quad (8a)$$

$$m_{22}^o = m_{22} - z_c n_{22} \quad (8b)$$

$$m_{12}^o = m_{12} - z_c n_{12} \quad (8c)$$

3) The following quantities do not vary through the thickness (with ξ_3):

$$N_{11}, \quad N_{22}, \quad N_{12}, \quad n_{11}, \quad n_{22}, \quad n_{12}, \quad q_1, \quad q_2, \quad \text{and } w$$

4) The applied in-plane stress resultants, N_{11} , N_{22} , and N_{12} act at the centroidal surface.

Substitution of Eqs. (7) and (8) into the original linear stability equations yields the following modified linear stability equations:

$$\begin{aligned} n_{11,1} + \hat{n}_{12,2} + \frac{q_1}{R_1} - \frac{N_{11}}{R_1} \left(w_{,1} - \frac{u_1 - z_c \phi_1}{R_1} \right) \\ - \frac{N_{12}}{R_1} \left(w_{,2} - \frac{u_2 - z_c \phi_2}{R_2} \right) - \underline{C}N_{11} \left(\frac{w}{R_1} + u_{1,1} - z_c \phi_{1,1} \right) \\ + \underline{G}N_{12} [u_2 - z_c \phi_2]_{,11} - \underline{H}N_{12} [u_1 - z_c \phi_1]_{,12} = 0 \end{aligned} \quad (9a)$$

$$\begin{aligned} n_{12,1} + \hat{n}_{22,2} + \frac{q_2}{R_2} - \frac{N_{22}}{R_2} \left(w_{,2} - \frac{u_2 - z_c \phi_2}{R_2} \right) \\ - \frac{N_{12}}{R_2} \left(w_{,1} - \frac{u_1 - z_c \phi_1}{R_1} \right) - \underline{B}N_{11} (u_2 - z_c \phi_2)_{,11} \\ + \underline{G}N_{12} \left(\frac{w_{,1}}{R_1} + [u_1 - z_c \phi_1]_{,11} \right) \\ - \underline{H}N_{12} \left(\frac{w_{,1}}{R_2} + [u_2 - z_c \phi_2]_{,12} \right) = 0 \end{aligned} \quad (9b)$$

$$\begin{aligned}
& q_{1,1} + \hat{q}_{2,2} - \frac{n_{11}}{R_1} - \frac{\hat{n}_{22}}{R_2} - N_{11} \left(w_{,1} - \frac{u_1 - z_c \phi_1}{R_1} \right)_{,1} \\
& - N_{12} \left(w_{,2} - \frac{u_2 - z_c \phi_2}{R_2} \right)_{,1} \\
& + \frac{CN_{11}}{R_1} \left(\frac{w}{R_1} + [u_1 - z_c \phi_1]_{,1} \right) \\
& + \frac{GN_{12}[u_2 - z_c \phi_2]_{,1}}{R_1} + \frac{HN_{12}[u_1 - z_c \phi_1]_{,2}}{R_1} = 0
\end{aligned} \tag{9c}$$

$$m_{11,1} + m_{12,2} - z_c(n_{11,1} + n_{12,2}) - q_1 = 0 \tag{9d}$$

$$m_{12,1} + m_{22,2} - z_c(n_{12,1} + n_{22,2}) - q_2 = 0 \tag{9e}$$

As will be discussed subsequently, a sinusoidal variation of the displacements and forces in the ξ_1 -direction will be assumed to simplify the analysis by reducing the linear stability equations to a system of ordinary differential equations. Therefore, the boundary conditions for an edge $\xi_1 = \text{constant}$ are ignored. The remaining natural boundary conditions for an edge $\xi_2 = \text{constant}$ are

$$\begin{aligned}
& \hat{n}_{12} = n_{12} - \underline{E}N_{22}[u_1 - z_c \phi_1]_{,2} \\
& + \underline{G}N_{12} \left([u_2 - z_c \phi_2]_{,2} + \frac{w}{R_2} \right) \\
& - \underline{H}N_{12} \left([u_1 - z_c \phi_1]_{,1} + \frac{w}{R_1} \right) = 0
\end{aligned} \tag{10a}$$

$$\begin{aligned}
& \hat{n}_{22} = n_{22} - \underline{F}N_{22} \left([u_2 - z_c \phi_2]_{,2} + \frac{w}{R_2} \right) \\
& + \underline{G}N_{12}[u_1 - z_c \phi_1]_{,2} \\
& - \underline{H}N_{12}[u_2 - z_c \phi_2]_{,1} = 0
\end{aligned} \tag{10b}$$

$$\begin{aligned}
& \hat{q}_2 = q_2 - N_{12} \left(w_{,1} - \frac{[u_1 - z_c \phi_1]}{R_1} \right) \\
& - N_{22} \left(w_{,2} - \frac{[u_2 - z_c \phi_2]}{R_2} \right) + [m_{12} - z_c n_{12}]_{,1}
\end{aligned} \tag{10c}$$

$$m_{12} - z_c n_{12} = 0 \tag{10d}$$

$$m_{22} - z_c n_{22} = 0 \tag{10e}$$

where the terms with a caret (^) are forces per unit length at an edge $\xi_2 = \text{constant}$ that are aligned with the original (undeformed) coordinates. These forces have been introduced herein because of the fact that the

stiffness matrix of a finite-strip element must relate the forces along the longitudinal edges of the plate in the original coordinate directions to the corresponding displacements along those edges. Note that the term $m_{12,1}$ which appears in the Kirchhoff shear term of CPT also appears in the expression for \hat{q}_2 for SDPT when γ_{13} is used as a fundamental displacement quantity.

Modified expressions for the last two stability equations are obtained by substituting expressions for the quantities $(n_{11,1} + n_{12,2})$ and $(n_{12,1} + n_{22,2})$ that are obtained by using Eqs. (9a) and (10a), and Eqs. (9b) and (10b) in the appropriate places in Eqs. (9d) and (9e), respectively. The definitions for the effective forces given in Eqs (10a)-(10c) are needed since the terms n_{12} and n_{22} that appear in the quantities in parentheses above are the perturbation values, not the effective forces. Substitution of the expressions for the two quantities in parentheses above into Eqs. (9d) and (9e), respectively, yields the final form of the last two stability equations

$$\begin{aligned}
& m_{11,1} + m_{12,2} - q_1 + z_c \left[\frac{q_1}{R_1} - \right. \\
& \left. \frac{N_{11}}{R_1} \left(w_{,1} - \frac{u_1 - z_c \phi_1}{R_1} \right) - \frac{N_{12}}{R_1} \left(w_{,2} - \frac{u_2 - z_c \phi_2}{R_2} \right) \right. \\
& \left. - \underline{C}N_{11} \left(\frac{w}{R_1} + u_{1,1} - z_c \phi_{1,1} \right)_{,1} - \underline{E}N_{22}(u_1 - z_c \phi_1)_{,22} \right. \\
& \left. + \underline{G}N_{12} \left(\frac{w_{,2}}{R_2} + [u_2 - z_c \phi_2]_{,11} + [u_2 - z_c \phi_2]_{,22} \right) \right. \\
& \left. - \underline{H}N_{12} \left(\frac{w_{,2}}{R_1} + 2[u_1 - z_c \phi_1]_{,12} \right) \right] = 0
\end{aligned} \tag{11a}$$

$$\begin{aligned}
& m_{12,1} + m_{22,2} - q_2 \\
& + z_c \left[\frac{q_2}{R_2} - \frac{N_{22}}{R_2} \left(w_{,2} - \frac{u_2 - z_c \phi_2}{R_2} \right) \right. \\
& \left. - \frac{N_{12}}{R_2} \left(w_{,1} - \frac{u_1 - z_c \phi_1}{R_1} \right) - \underline{B}N_{11}(u_2 - z_c \phi_2)_{,11} \right. \\
& \left. - \underline{F}N_{22} \left(\frac{w_{,2}}{R_2} + [u_2 - z_c \phi_2]_{,22} \right) \right. \\
& \left. + \underline{G}N_{12} \left(\frac{w_{,1}}{R_1} + [u_1 - z_c \phi_1]_{,11} + [u_1 - z_c \phi_1]_{,22} \right) \right. \\
& \left. - \underline{H}N_{12} \left(\frac{w_{,1}}{R_2} + 2[u_2 - z_c \phi_2]_{,12} \right) \right] = 0
\end{aligned} \tag{11b}$$

These modified equations are used to simplify the numerical procedure used to implement the present analysis into the VICONOPT code. The stability equations in the form given in Eqs. (9a)-(9c) and Eqs.

(11a)-(11b) are those implemented into the VICONOPT code.

Constitutive Relations

The through-the-thickness geometry and the geometry of an arbitrary lamina of a general, curved laminate is given in Figure 5. The number of layers in the laminate is n_l , and as shown in the figure, the arc-width of the laminate is b . The ξ_1 - and ξ_2 -axes are the principal material axes of the k th specially orthotropic lamina that makes an angle θ_k with the ξ_1 -axis in the middle surface tangent plane at a given point of the plate. The laminate ξ_1 -axis is aligned with the longitudinal edges of the plate. The overall isothermal constitutive relations for a thin, elastic laminated composite shell are defined in reference [17] as

$$\begin{Bmatrix} \mathbf{N} \\ \mathbf{M} \end{Bmatrix} = \begin{bmatrix} \mathbf{A} & \mathbf{B} \\ \mathbf{B} & \mathbf{D} \end{bmatrix} \begin{Bmatrix} \boldsymbol{\varepsilon} \\ \boldsymbol{\kappa} \end{Bmatrix} \quad (12)$$

The stress and moment resultants acting on the laminate, $\{\mathbf{N}\}$ and $\{\mathbf{M}\}$, respectively, are defined as

$$\begin{Bmatrix} N_{11} \\ N_{22} \\ N_{12} \end{Bmatrix} = \sum_{k=1}^{n_l} \int_{z_{k-1}}^{z_k} \begin{Bmatrix} \sigma_{11} \\ \sigma_{22} \\ \tau_{12} \end{Bmatrix} d\xi_3 \quad (13)$$

$$\begin{Bmatrix} M_{11} \\ M_{22} \\ M_{12} \end{Bmatrix} = \sum_{k=1}^{n_l} \int_{z_{k-1}}^{z_k} \begin{Bmatrix} \sigma_{11} \\ \sigma_{22} \\ \tau_{12} \end{Bmatrix} \xi_3 d\xi_3 \quad (14)$$

The extensional, coupling, and bending stiffness matrices, \mathbf{A} , \mathbf{B} , and \mathbf{D} , respectively, are defined as

$$(\mathbf{A}, \mathbf{B}, \mathbf{D}) = \sum_{k=1}^{n_l} \int_{z_{k-1}}^{z_k} [\bar{\mathbf{Q}}^k] \begin{pmatrix} 1, & \xi_3, & \xi_3^2 \end{pmatrix} d\xi_3 \quad (15)$$

The constitutive relations for transverse shear used in VICONOPT are those presented by Cohen in [14]. The constitutive relations for transverse shear are written in inverted form as

$$\begin{Bmatrix} \gamma_{13} \\ \gamma_{23} \end{Bmatrix} = \begin{bmatrix} k_{11} & k_{12} \\ k_{12} & k_{22} \end{bmatrix} \begin{Bmatrix} q_1 \\ q_2 \end{Bmatrix} \quad (16)$$

where $[\mathbf{k}]$ is a symmetric 2-by-2 transverse shear compliance matrix whose terms are defined in [14].

Implementation into VICONOPT

The implementation of the present theory into the VICONOPT code is described in this section. Several simplifications made to the present theory are described first. Then the derivation of the curved-plate stiffness matrix based upon the analysis of the present study is presented. The implementation of the present curved-

plate theory into VICONOPT follows very closely the procedure described in [2]. Therefore, for convenience, the following discussion is presented in a form similar to that in [2].

Simplifications to the Theory

The theory implemented into the VICONOPT code is for structures that are prismatic in the longitudinal direction. Therefore, for the curved-plate elements that are considered in the present paper, the radius of curvature in the longitudinal direction, R_1 , is infinite; i.e., any terms involving the quantity $\frac{1}{R_1}$ are zero.

Although these terms are set equal to zero in the calculation of the terms of the stiffness matrix, they have been retained for completeness of the theory presented herein. Another simplification to the theory involves limiting the capability to locate the reference surface a distance z_c from the centroidal surface. This capability has only been implemented for the case where the effects of N_{22} and N_{12} loads in the in-plane stability equations are neglected. The expressions for the stiffness terms that result when N_{22} and N_{12} are included in the in-plane stability equations are prohibitively long. Therefore, in the derivation of the stiffness matrix that follows, only the following two cases are included:

1) N_{22} and N_{12} are included in the in-plane stability equations and z_c is zero (i.e., reference surface is coincident with the centroidal surface)

2) N_{22} and N_{12} are neglected in the in-plane stability equations and z_c is non-zero (i.e., reference surface may be shifted from the centroidal surface)

Derivation of the Curved-Plate Stiffness Matrix

Throughout this section, reference is made to force quantities. Although these quantities are force per unit length, they are designated forces herein for convenience. The first step in implementing the present theory into VICONOPT is to derive a stiffness matrix that relates the force quantities along the two longitudinal edges (referred to herein as simply forces), $\xi_2 = \pm \frac{b}{2}$, to the displacements along those edges. The desired force and displacement quantities are in the direction of the original (undeformed) coordinates. The displacement and force variables are

$$\mathbf{d} = \begin{Bmatrix} i & u_1 \\ & u_2 \\ & w \\ & \phi_2 \\ i & \gamma_{13} \end{Bmatrix} \quad \text{and} \quad \mathbf{f} = \begin{Bmatrix} i & \hat{n}_{12} \\ & \hat{n}_{22} \\ & \hat{q}_2 \\ & m_{22} \\ i & m_{12} \end{Bmatrix} \quad (17)$$

where the shear strain, γ_{13} , has been introduced as a fundamental displacement quantity instead of the rotation, ϕ_1 . Note that the effective forces per unit length at the boundaries, defined by Eqs. (10a)-(10c), are used as forces since they are equal to forces in the direction of the original (undeformed) coordinates.

The curved-plate element equations may now be reduced to ordinary differential equations in ξ_2 by assuming that the response of the plate in the longitudinal ξ_1 -direction varies sinusoidally. For isotropic or orthotropic plate assemblies without shear loading, a sinusoidal response in the ξ_1 -direction is exact for simply supported end conditions. A series of sinusoidal modes is used with a Lagrangian multiplier technique to obtain results for other loadings and end conditions [2]. Applying the assumption of a sinusoidal variation in the ξ_1 -direction, the variables of Eqs. (17) may be written as

$$\mathbf{Z}(\xi_1, \xi_2) = \exp\left(\frac{i \pi \xi_1}{\lambda}\right) \mathbf{z}(\xi_2), \quad \mathbf{z} = \begin{Bmatrix} \mathbf{d} \\ \mathbf{f} \end{Bmatrix} \quad (18)$$

where λ is the half-wavelength of the response in the ξ_1 -direction. Since a sinusoidal variation in the ξ_1 -direction is assumed, the vector \mathbf{z} will involve the amplitudes of the displacement and forces. The imaginary number, i , has been used in Eqs. (17) to account for the spatial phase shift that occurs between the displacement and force quantities when an in-plane shear loading is present and to result in real plate stiffnesses when using the exponential expression of Eq. (18).

The next step in the derivation is to express all unknowns in terms of \mathbf{z} . A partially inverted form of the constitutive relations is used to express the required quantities as functions of the fundamental variables in \mathbf{d} and \mathbf{f} , or terms that may be derived from the fundamental variables. The partially inverted constitutive relations are given in reference [2].

Another requirement of the present derivation is to express the relationship between q_2 and \hat{q}_2 without any ξ_2 -derivatives so that a first-order system of differential equations is maintained. This expression is

$$q_2 = \frac{\begin{pmatrix} \hat{q}_2 + N_{12} \left(w_{,1} - \frac{[u_1 - z_c \phi_1]}{R_1} \right) \\ + N_{22} (\phi_2 - h_{78} \gamma_1) + [m_{12} - z_c n_{12}]_{,1} \end{pmatrix}}{1 - N_{22} h_{88}} \quad (19)$$

where h_{78} and h_{88} are terms from the partially inverted constitutive relations given in reference [2]. As with the stability equations, only the linear portion of the strain-displacement relations (Eqs. (2c), (2b), (2e), (3b), and (3c)) are considered in the present derivation. The

expression for κ_{12} is re-written after substituting expressions obtained for ϕ_1 and ϕ_2 from Eqs. (2d) and (2e) and using the linear portion of ϵ_{12} , that is,

$$\kappa_{12} = - \left[\gamma_2 + \left(\frac{1}{R_1} + \frac{1}{R_2} \right) u_2 + 2\phi_2 \right]_{,1} + \frac{\epsilon_{12}}{R_1} + \gamma_{1,2} \quad (20)$$

Using the partially inverted constitutive relations and Eq. (19), the strain displacement equations, Eqs. (2c), (2b), (2e), (3b), and (3c), and the stability equations, Eqs. (9a)-(9c) and Eqs. (11a) and (11b) are written in terms of the elements of \mathbf{z} as

$$\mathbf{T} \mathbf{z}' = \mathbf{P} \mathbf{z} \quad \text{or} \quad \mathbf{z}' = \mathbf{T}^{-1} \mathbf{P} \mathbf{z} \quad (21)$$

where a prime denotes differentiation with respect to ξ_2 . The square matrix \mathbf{T} appears in the present study as a result of the inclusion of the effects of N_{22} and N_{12} in the in-plane stability equations. When these terms are neglected, this matrix is shown to be the identity matrix in reference [2]. The use of the modified stability equations given in Eqs. (11a) and (11b) is also required for \mathbf{T} to be the identity matrix. The presence of off-diagonal terms in \mathbf{T} is a fundamental difference between the present theory and that presented in reference [2].

The elements of \mathbf{z} are now assumed to be given by

$$z_j = c_j \exp\left(\frac{i \beta \xi_2}{b}\right) \quad (22)$$

where β is a characteristic root of the system of differential equations. The number of values of β is equal to the order of the differential equation system. Substituting Eq. (22) into Eq. (21) results in the following equation

$$(\mathbf{R} - \beta \mathbf{I}) \mathbf{c} = 0, \quad \text{where} \quad \mathbf{R} = b \mathbf{T}^{-1} \mathbf{P} \quad (23)$$

where \mathbf{I} is the identity matrix. The vector \mathbf{c} consists of the c_j of Eq. (22). The eigenvalues of the matrix \mathbf{R} are the characteristic roots of the differential equation. This matrix is not symmetric; however, it can be made real by multiplication or division of appropriate rows and columns by the imaginary number, i . The elements of the matrices \mathbf{T} and \mathbf{P} are given in reference [16]. For each eigenvalue of \mathbf{R} , there exists an eigenvector, \mathbf{c} . The upper half of each eigenvector, denoted \mathbf{a} , is associated with displacements, and the lower half, denoted \mathbf{b} , is associated with forces.

The next step in the derivation is to determine the amplitudes of the displacements and forces at the two edges of the plate. Quantities evaluated at $\xi_2 = -\frac{b}{2}$ are identified with a superscript 1 and quantities

evaluated at $\xi_2 = +\frac{b}{2}$ are identified with a superscript 2 as follows:

$$d_j^1 = \sum_{k=1}^N a_{jk} r_k \exp\left(\frac{-i \beta_k}{2}\right) \quad (24a)$$

$$d_j^2 = \sum_{k=1}^N a_{jk} r_k \exp\left(\frac{i \beta_k}{2}\right) \quad (24b)$$

$$f_j^1 = \sum_{k=1}^N b_{jk} r_k \exp\left(\frac{-i \beta_k}{2}\right) \quad (24c)$$

$$f_j^2 = \sum_{k=1}^N b_{jk} r_k \exp\left(\frac{i \beta_k}{2}\right) \quad (24d)$$

where the r_k are constants determined from the edge values and N is the order of the system of differential equations. Equations (24a)-(24d) may be written in matrix form as

$$\begin{Bmatrix} \mathbf{d}^1 \\ \mathbf{d}^2 \end{Bmatrix} = \mathbf{E} \mathbf{r} \quad \text{and} \quad \begin{Bmatrix} \mathbf{f}^1 \\ \mathbf{f}^2 \end{Bmatrix} = \mathbf{F} \mathbf{r} \quad (25)$$

Eliminating \mathbf{r} from Eqs. (25) yields

$$\begin{Bmatrix} \mathbf{f}^1 \\ \mathbf{f}^2 \end{Bmatrix} = \mathbf{K} \begin{Bmatrix} \mathbf{d}^1 \\ \mathbf{d}^2 \end{Bmatrix} \quad (26)$$

where \mathbf{K} is the stiffness matrix given by

$$\mathbf{K} = \mathbf{F} \mathbf{E}^{-1} \quad (27)$$

For CPT, \mathbf{K} is real and symmetric. For SDPT, \mathbf{K} is real and symmetric for orthotropic plates without in-plane shear loading, and it is Hermitian otherwise. Reference [2] presents a discussion of techniques used to ensure that accurate numerical results for \mathbf{K} are obtained from Eq. (27). The stiffness matrix \mathbf{K} is a transcendental function of the load factor and half wavelength of the buckling modes of the structure. Therefore, the eigenvalue problem for determining bifurcation buckling load factors is transcendental. The iterative analysis procedure used in VICONOPT to solve this eigenvalue problem is based upon the Wittrick-Williams eigenvalue algorithm described in [18]. This algorithm will not be discussed in the present paper.

Numerical Results

Numerical results are presented in this section that were obtained using the new curved-plate analysis derived herein that has been implemented into the VICONOPT code. Results for several known example problems are presented to verify the results obtained with this new capability. Comparisons of analyses that use both physical and tensorial strain measures are made for selected examples, and, where appropriate,

results based upon CPT and SDPT are compared. The positive sense of the applied loadings for all of the following examples is given in Figure 6.

Convergence of the Segmented-Plate Approach

The convergence of bifurcation buckling results obtained using the segmented-plate analysis in VICONOPT is examined for the long, compression-loaded aluminum cylinder illustrated in Figure 7. The values of the material properties used for this example are $E = 10.0 \times 10^6$ psi and $\nu_{12} = 0.33$. The wall thickness, t , is 0.1 in., and the radius, R_2 is 60 in. As shown in Ref. [19], the critical value for the applied stress resultant, $(N_{11})_{cr}$, for the axisymmetric buckling of a long isotropic cylindrical shell is

$$(N_{11})_{cr} = \frac{Et^2}{R_2 \sqrt{3(1-\nu^2)}} = 1019.354 \text{ lb/in.} \quad (28)$$

and the corresponding critical half wavelength, λ_{cr} , is

$$\lambda_{cr} = \pi \sqrt[4]{\frac{R_2^2 t^2}{12(1-\nu^2)}} = 1.74 \sqrt{R_2 t} = 4.255 \text{ in.} \quad (29)$$

Results that illustrate the convergence of the VICONOPT segmented-plate results for $(N_{11})_{cr}$ as a function of the number of flat-plate elements used to approximate the cylinder are shown in Figure 8. In this figure, the results of the segmented-plate analysis are shown as the solid curve. The theoretical value obtained from Ref. [19] is shown as the dashed horizontal line. The value obtained by using the present curved-plate analysis is shown as the open symbol. All results in this figure were calculated for the value of λ_{cr} given in Eq. (29). The VICONOPT results presented in this figure were obtained using CPT with tensorial strain measures. As shown in Figure 8, the segmented-plate results converge to the theoretical value of 1019.354 lb/in. when 120 flat-plate elements are used. Therefore, to ensure that converged results are obtained when the segmented-plate approach is used to analyze the remaining example problems, sixty elements will be used when analyzing curved plates with an included angle of 180 degrees or less, and 120 elements will be used when analyzing full cylinders.

Buckling of an Unsymmetrically Laminated Curved Plate

This example problem includes the effect of bending-stretching coupling and shear-extension coupling on the buckling of an unsymmetrically laminated curved plate with simply supported

longitudinal edges (i.e., $u_1 = w = m_{22} = 0$). The pre-buckling deformations associated with bending-stretching coupling are neglected in the analysis. The geometry of the curved plate is shown in Figure 9. To allow for direct comparison of results with those presented in [6], SI units are used. As shown in the figure, the laminate that is being studied consists of a 0.508-cm.-thick layer of 2024 aluminum that is reinforced on the inner surface with pairs of $\pm 45^\circ$ boron/epoxy plies. The material properties for a boron/epoxy lamina and 2024 aluminum are given in Table 1. For this example, the number of pairs of $\pm 45^\circ$ boron/epoxy plies is increased from one to seven. Both physical and tensorial strains are used with the new curved-plate analysis, while only physical strains are used with the segmented-plate analysis. The analysis of [6] uses physical strains. All analyses use CPT. Eight curved-plate elements are used for the curve-plate analyses, and 60 flat-plate elements are used for the segmented-plate analysis. The critical value of the applied stress resultants N_{11} and N_{12} at buckling are plotted as a function of the number of boron/epoxy plies used in the laminate in Figure 10 and Figure 11, respectively. The agreement between all the analyses is very good. As shown in the figures, there is no appreciable difference in the results obtained using physical and tensorial strains.

Design Optimization of a Cylindrical Shell Subject to Uniaxial Compression

The final example utilizes the new curved-plate analysis with the design optimization capability of VICONOPT to perform a structural optimization of two different cylindrical shell concepts subject to uniform axial compression (N_{11} loading). The two concepts are solid-wall construction and honeycomb-sandwich-wall construction. The geometry of this example problem is shown in Figure 12. As shown in the figure, the facesheets of the honeycomb-sandwich-wall concept are aluminum, and the core is KorexTM aramid paper honeycomb core [20]. The solid-wall concept is aluminum. The material properties used for the facesheets and core are presented in Table 2. Tensorial strains are used for the analysis.

The design variables for the structural optimization are the thicknesses of the facesheets and the core for the sandwich concept and the wall thickness for the solid-wall construction. There is no minimum gage restriction on these design variables. The nominal values for these variables are 0.1 in., 0.5 in., and 0.1 in., respectively. The design constraints are that the strain in the facesheets or the solid wall cannot exceed 0.005 in/in and that the stress in the core cannot exceed 115 psi in the ξ_1 direction and 55 psi in the ξ_2 direction.

The results of this study, including the mass of the optimized cylinder and the final values of the design variables are given in Table 3 for the honeycomb-sandwich-wall concept and in Table 4 for the solid-wall concept. Results obtained using both CPT and SDPT with tensorial strains are given in these tables. The optimized mass values are also plotted as a function of the applied loading in Figure 13. As seen in the tables and the figure, the values of the optimized mass obtained using CPT are slightly less than those for SDPT for the honeycomb-sandwich-wall cylinder as the applied loading is increased. However, the values of the core thickness obtained using CPT become significantly less than those for SDPT as the loading is increased. This trend is expected because CPT results in an overly stiff approximation since transverse-shear flexibility is neglected. This overly stiff approximation results in higher buckling loads for a given core thickness. Therefore, the core thickness and the optimum mass obtained using CPT is less than that obtained using SDPT. The optimized mass values for the solid-wall construction are much greater than those for the honeycomb sandwich construction. The results for CPT and SDPT are nearly identical for the solid-wall construction with $R_2/t = 600$, as expected.

Concluding Remarks

The VICONOPT computer code is an exact analysis and optimum design program that includes the buckling and vibration analyses of prismatic assemblies of flat, in-plane-loaded anisotropic plates. In the present paper, the capability to analyze structures by using curved-plate elements has been described, and this capability has been added to the VICONOPT code. Non-linear curved-plate equilibrium equations have been formulated, and linearized stability equations were derived following the application of several simplifying assumptions. Modifications to these equations were then made to allow the reference surface of the plate to be located at a distance z_c from the centroidal surface.

The analysis described in the present paper improves upon the analysis existing previously in the VICONOPT code which required that curved-plate geometries be subdivided into several flat-plate elements that are joined along their longitudinal edges to approximate the curved-plate geometry. The new analysis formulation includes either classical plate theory (CPT) and first-order shear-deformation plate theory (SDPT), and anisotropic laminates with fully populated **A**, **B**, and **D** stiffness matrices can be analyzed.

The option to use plate elements (flat or curved) that are based upon nonlinear strain-displacement

relations that contain terms from either physical or tensorial strain measures has also been added to the VICONOPT code. The option to include the effect of terms associated with in-plane transverse and in-plane shear loading in the in-plane stability equations has been added as well.

Results from the present curved-plate analysis capability compare very well with a closed-form solution and the existing segmented-plate analysis for the linear bifurcation buckling of a long isotropic cylinder subjected to uniaxial compression. Results from the present analysis also compare well with results for unsymmetrically laminated plates that include the effect of extension-bending and shear-extension coupling. No appreciable effects of using tensorial versus physical strains were noted in these examples.

Finally, the present curved-plate analysis was used to conduct a design-optimization study of two cylindrical shells subject to uniform axial compression. One shell was constructed with a honeycomb-sandwich-wall, and the other was a solid-wall construction. The values of mass for the optimized solid-wall design were much higher than those for the honeycomb-sandwich-wall construction. There was no difference between results using CPT and SDPT for the solid-wall cylinder. However, the values of core thickness and mass for the optimized honeycomb-sandwich-wall cylinder using CPT were less than those for SDPT as the applied loading was increased. This result occurred because CPT overestimates the wall stiffness by neglecting transverse-shear flexibility which results in higher buckling loads and a lower optimum mass.

References

1. Williams, F. W., Kennedy, D., Anderson, M. S., and Edwards, D. A., "User Manual for VICONOPT," Release 1.3, April 1996.
2. Anderson, M. S., and Kennedy, D., "Inclusion of Transverse Shear Deformation in the Exact Buckling and Vibration Analysis of Composite Plate Assemblies," Presented at the AIAA/ASME/ASCE/AHS/ACE 32nd Structures, Structural Dynamics and Materials Conference, Dallas, Texas, April 13-15, 1992. AIAA Paper No. 92-2287.
3. Cheung, Y. K., *The Finite Strip Method in Structural Analysis*, Pergamon Press, Oxford, England, 1976.
4. Viswanathan, A. V., and Tamekuni, M., "Elastic Buckling Analysis For Composite Stiffened Panels and other Structures Subjected to Biaxial Inplane Loads," NASA CR-2216, 1973.
5. Viswanathan, A. V., Tamekuni, M., and Tripp, L. L., "Elastic Stability of Biaxially Loaded Longitudinally Stiffened Composite Structures," Proceedings of the AIAA/ASME/SAE 14th Structures, Structural Dynamics, and Materials Conference, Williamsburg, VA, March 20-22, 1973. AIAA Paper No. 73-367.
6. Viswanathan, A. V., Tamekuni, M., and Baker, L. L., "Elastic Stability of Laminated, Flat and Curved, Long Rectangular Plates Subjected to Combined Loads," NASA CR-2330, 1974.
7. Dawe, D. J., "Finite Strip Buckling Analysis of Curved Plate Assemblies Under Biaxial Loading," *International Journal for Numerical Methods in Engineering*, Vol. 13, 1977, pp. 1141-1155.
8. Morris, I. R., and Dawe, D. J., "Free Vibration of Curved-Plate Assemblies With Diaphragm Ends," *Journal of Sound and Vibration*, Vol. 73, 1980, pp. 1-17.
9. Novozhilov, V. V., *Foundations of the Nonlinear Theory of Elasticity*, Graylock Press, Rochester, New York, 1963.
10. Stein, M., "Nonlinear Theory for Plates and Shells Including the Effects of Transverse Shearing," *AIAA Journal*, Vol. 24, No. 9, September 1986, pp. 1537-1544.
11. Sanders, J. L., Jr., "Nonlinear Theories for Thin Shells," *Quarterly of Applied Mathematics*, Vol. 21, 1963, pp. 21-36.
12. Shames, I. H., and Dym, C. L., *Energy and Finite Element Methods in Engineering Mechanics*, Hemisphere Publishing Corporation, New York, New York, 1985.
13. Sanders, J. L., Jr., "An Improved First-Approximation Theory For Thin Shells," NASA TR R-24, 1959.
14. Cohen, G. A., "Transverse Shear Stiffness of Laminated Anisotropic Shells," *Computer Methods in Applied Mechanics and Engineering*, Vol. 13, 1978, pp. 205-220.
15. Cohen, G. A., "FASOR - A Second Generation Shell of Revolution Code," *Computers & Structures*, Vol. 10, 1979, pp. 301-309.
16. McGowan, D. M., "Development Of Curved-Plate Elements For The Exact Buckling Analysis Of Composite Plate Assemblies Including Transverse Shear Effects," M.S. Thesis, Old Dominion University, Norfolk, VA, to appear May, 1997.
17. Jones, R. M., *Mechanics of Composite Materials*, Hemisphere Publishing Corp., New York, New York, 1975.

18. Wittrick, W. H., and Williams, F. W., “An Algorithm for Computing Critical Buckling Loads of Elastic Structures,” *Journal of Structural Mechanics*, Vol. 1, 1973, pp. 497-518.
19. Timoshenko, S. P., and Gere, J. M., *Theory of Elastic Stability, Second Edition*, McGraw-Hill Book Company, New York, New York, 1961.
20. Anonymous, DuPont KOREX™ Honeycomb Core for High Performance Applications, DuPont Technical Data Specification Sheet.

Table 1. Material properties for boron/epoxy plies and 2024 aluminum (SI units).

Material	$E_{11} \times 10^{-10}$, N/m ²	$E_{22} \times 10^{-10}$, N/m ²	$G_{12} \times 10^{-10}$, N/m ²	ν_{12}	ρ , kg/m ³
Boron/epoxy	20.69	1.86	0.48	0.21	2006.8
Aluminum 2024	7.38	7.38	2.76	0.33	2768.0

Table 2. Material properties for aluminum and Korex™ honeycomb core (English Engineering units).

Material	$E_{11} \times 10^{-6}$, lb/in ²	$E_{22} \times 10^{-6}$, lb/in ²	$G_{12} \times 10^{-6}$, lb/in ²	$G_{13} \times 10^{-6}$, lb/in ²	$G_{23} \times 10^{-6}$, lb/in ²	ν_{12}	ρ , lb/in ³
Aluminum	10.0	10.0	3.846	3.846	3.846	0.3	0.1
Korex™ H/C core	0.0001	0.0001	0.0001	0.012	0.004	0.3	0.00116

Table 3. Design-optimization results for a honeycomb sandwich cylinder subjected to N_{11} loading.

N_{11} , lb/in.	Classical plate theory (tensorial strains)			Transverse shear plate theory (tensorial strains)		
	t_{fs} , in.	t_{core} , in.	mass, lb _m	t_{fs} , in.	t_{core} , in.	mass, lb _m
1,000	0.010	0.310	213.53	0.010	0.313	213.85
2,000	0.020	0.334	397.00	0.020	0.338	397.43
3,000	0.030	0.324	576.88	0.030	0.331	577.64
4,000	0.040	0.280	753.17	0.040	0.349	760.47
5,000	0.050	0.270	933.02	0.050	0.367	943.44
10,000	0.100	0.250	1,835.8	0.100	0.606	1,873.2
15,000	0.150	0.194	2,734.7	0.150	0.909	2,809.7
20,000	0.200	0.135	3,633.3	0.200	1.212	3,746.3

Table 4. Design-optimization results for a solid-wall cylinder subjected to N_{11} loading.

N_{11} , lb/in.	Classical plate theory (tensorial strains)		Transverse shear plate theory (tensorial strains)	
	t_{wall} , in.	mass, lb _m	t_{wall} , in.	mass, lb _m
1,000	0.102	924.68	0.102	924.69
2,000	0.143	1,296.8	0.143	1,296.8
3,000	0.179	1,622.0	0.179	1,622.0
4,000	0.207	1,873.8	0.207	1,873.9
5,000	0.230	2,082.1	0.230	2,082.2
10,000	0.324	2,931.8	0.324	2,931.9
15,000	0.409	3,697.5	0.409	3,697.7
20,000	0.474	4,291.3	0.474	4,291.6

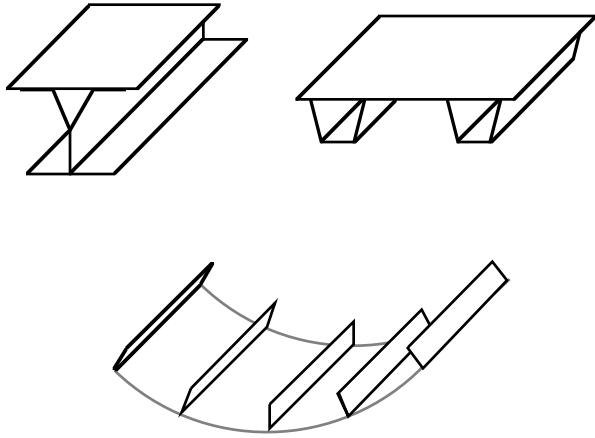


Figure 1. Typical longitudinally stiffened plate structures.

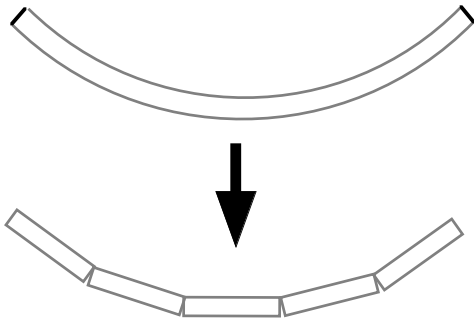


Figure 2. Segmented representation of curved-plate geometry currently used by VICONOPT.

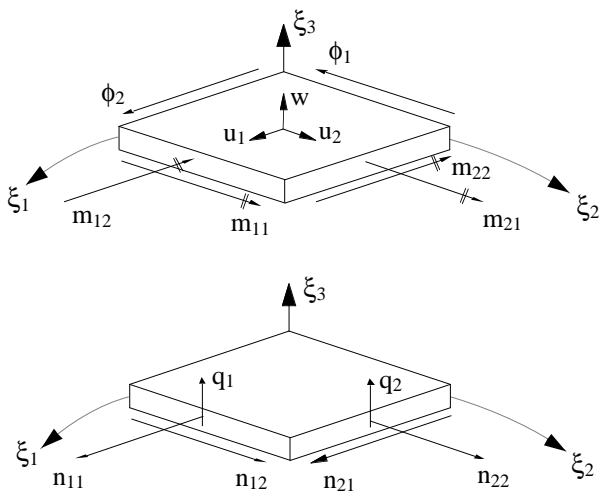


Figure 3. Curved-plate geometry and sign convention for buckling displacements, rotations, moments, and forces.

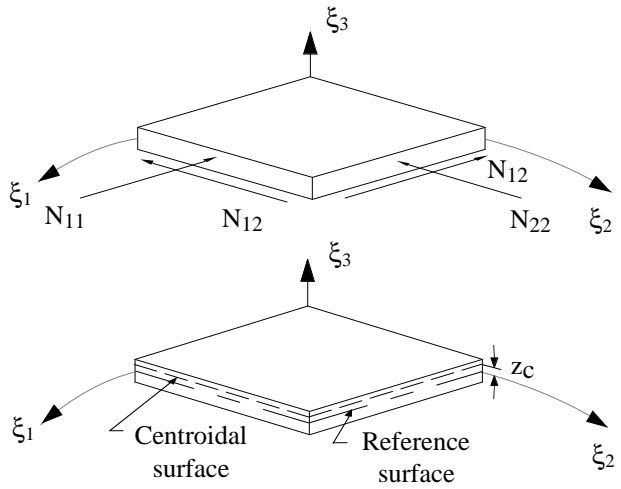


Figure 4. Sign convention for applied in-plane loads and relation of reference surface to centroidal surface.

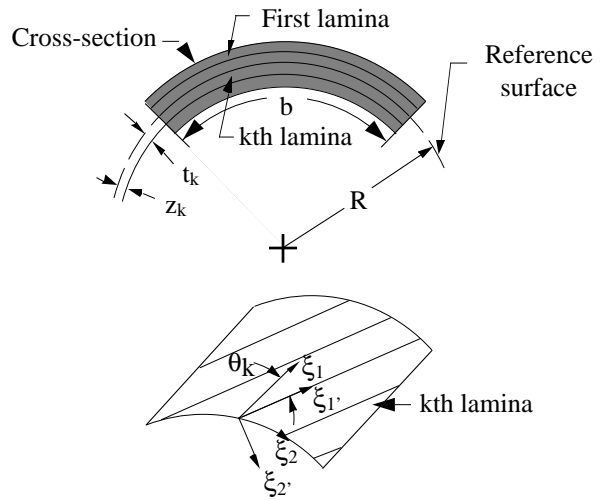


Figure 5. Curved-laminate geometry.

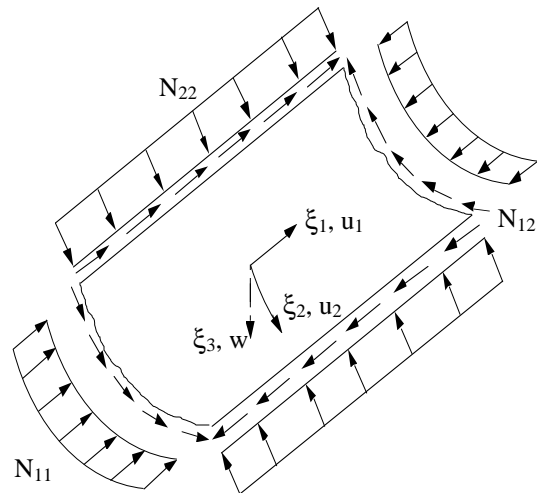
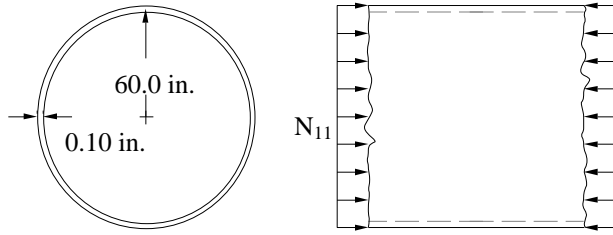


Figure 6. Positive applied in-plane loads on a long curved plate.



$E = 10.0 \times 10^6 \text{ psi}$
 $\nu_{12} = 0.33$
 $\rho = 0.1 \text{ lb/in}^3$

Figure 7. Long isotropic (aluminum) cylinder subjected to uniaxial compression.

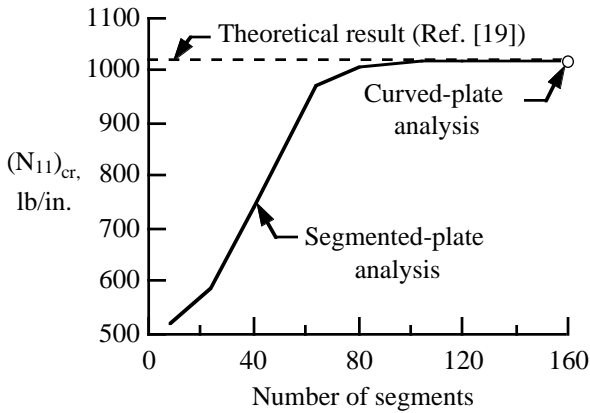


Figure 8. Convergence of VICONOPT segmented-plate results as a function of the number of elements used in the approximation.

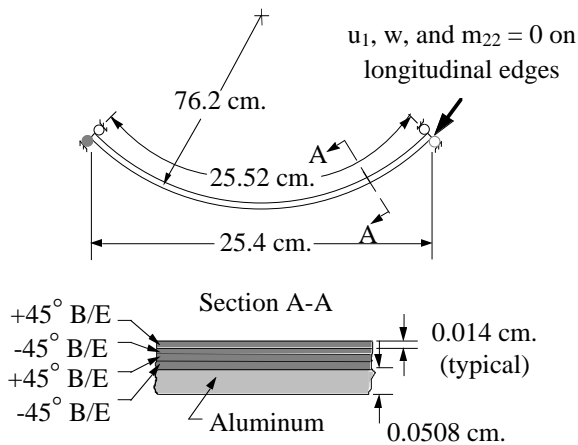


Figure 9. Unsymmetrically laminated curved plate with simply supported edges subjected to applied in-plane loads.

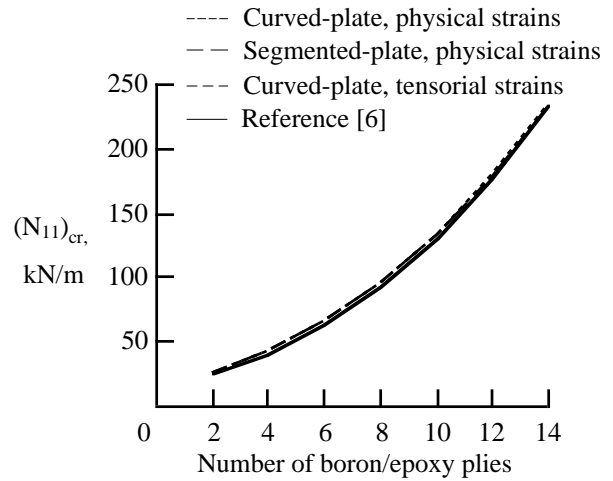


Figure 10. Critical value of N_{11} for buckling of an unsymmetrically laminated curved plate with simply supported longitudinal edges.

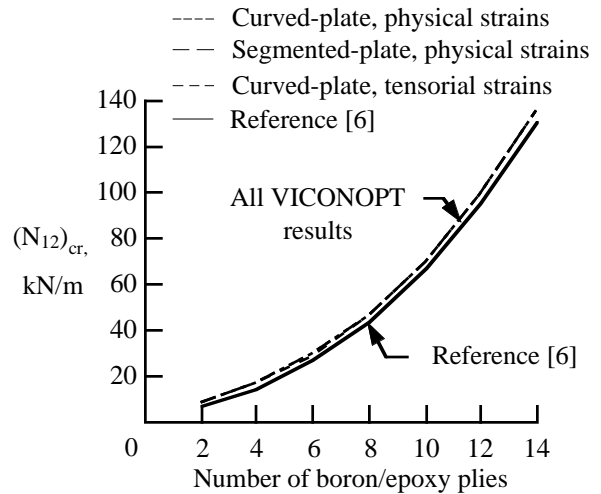


Figure 11. Critical value of N_{12} for buckling of an unsymmetrically laminated curved plate with simply supported longitudinal edges.

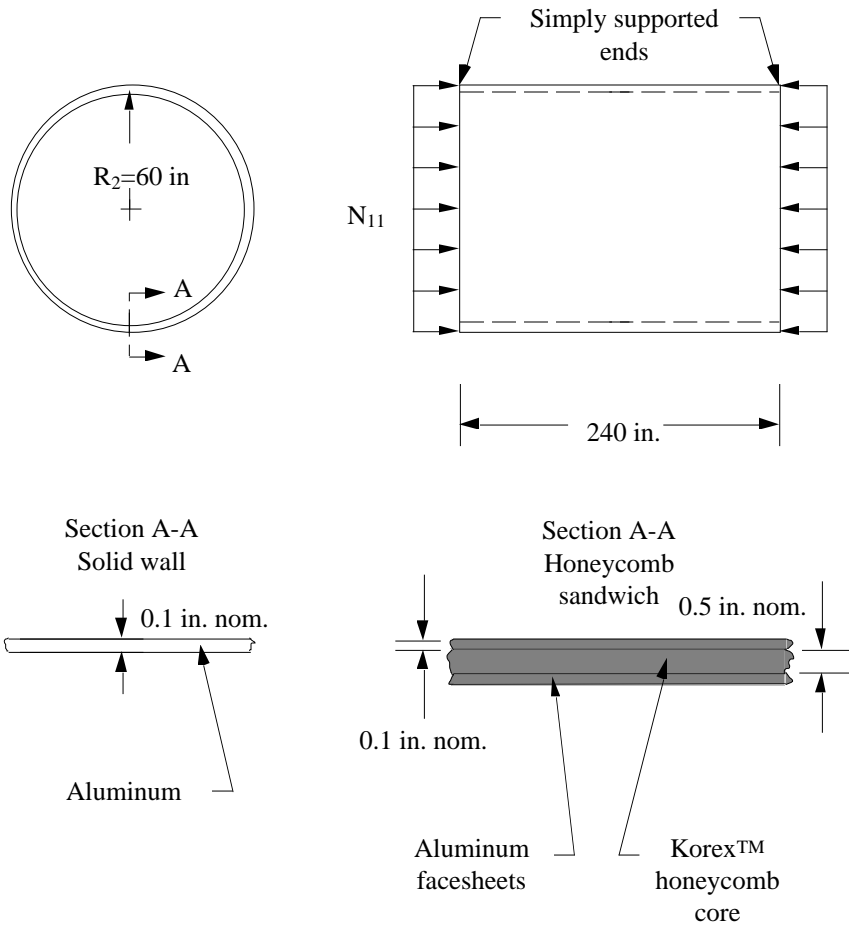


Figure 12. Cylindrical shell subjected to uniform axial compression (N_{11} loading).

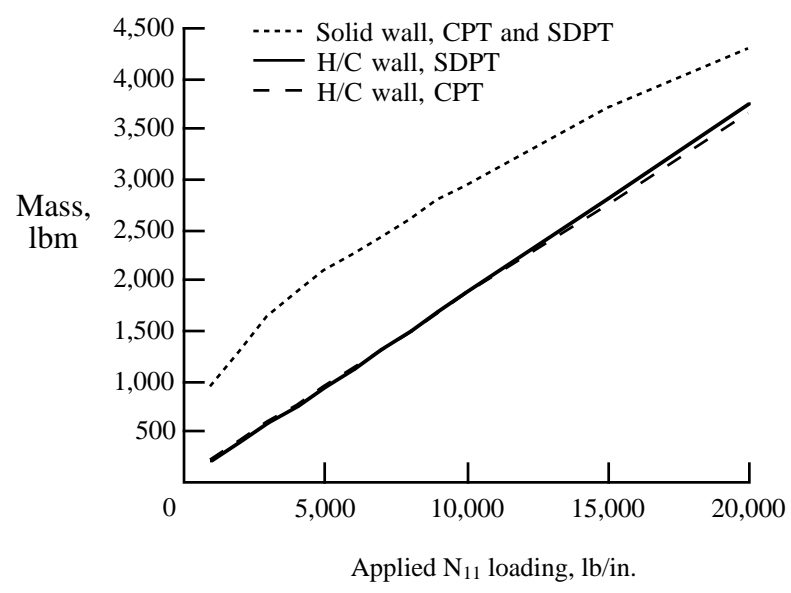


Figure 13. Optimized cylinder mass as a function of the applied loading for a cylindrical shell.